JACS
JOURNAL OF THE AMERICAN CHEMICAL SOCIETY
Communication
pubs.acs.org/JACS

Antimony-Based Ligand Exchange To Promote Crystallization in Spray-Deposited $Cu_2ZnSnSe_4$ Solar Cells

Alex Carrete,[†] Alexey Shavel,[†] Xavier Fontané,[†] Joana Montserrat,[‡] Jiandong Fan,[†] Maria Ibáñez,[†] Edgardo Saucedo,[†] Alejandro Pérez-Rodríguez,[†,‡] and Andreu Cabot*[,†,‡]

[†]Catalonia Energy Research Institute - IREC, Jardí de les Dones de Negre 1, Sant Adria del Besos, Barcelona, 08930, Spain
[‡]Departament d'Electrònica, Universitat de Barcelona, Barcelona 08028, Spain

Supporting Information

ABSTRACT: A multistrategy approach to overcome the main challenges of nanoparticle-based solution-processed $Cu_2ZnSnSe_4$ thin film solar cells is presented. We developed an efficient ligand exchange strategy, using an antimony salt, to displace organic ligands from the surface of Cu_2ZnSnS_4 nanoparticles. An automated pulsed spray-deposition system was used to deposit the nanoparticles into homogeneous and crack-free films with controlled thickness. After annealing the film in a Se-rich atmosphere, carbon-free and crystalline $Cu_2ZnSnSe_4$ absorber layers were obtained. Not only was crystallization promoted by the complete removal of organics, but also Sb itself played a critical role. The Sb-assisted crystal growth is associated with the formation of a Sb-based compound at the grain boundaries, which locally reduces the melting point, thus promoting the film diffusion-limited crystallization.

Cu_2ZnSnS_4 (CZTS) and $Cu_2ZnSnSe_4$ (CZTSe), composed of abundant and low-toxicity elements, are the main alternative to conventional absorber materials in thin film solar cells. CZTS and CZTSe thin films can be produced by conventional vacuum-based technologies, such as sputtering, evaporation or pulsed laser deposition. However, these technologies are neither particularly low-cost nor versatile for the production of large area devices, because of the relatively high energies and controlled atmospheres they require and the low growth rates and material yields they have associated. Alternative low cost solution-processing methods allow the preparation of large area thin film semiconductors at low temperatures and at high production rates and yields. Unprecedentedly, for CZTS/CZTSe solar cells, solution-processing technologies have also achieved significantly higher device efficiencies than conventional vacuum-based technologies.[1] This improved performance is associated with the excellent compositional and phase control achieved by solution-based methods in such complex quaternary materials.[2]

Nevertheless, solution-based technologies are not without limitations. The main challenges still encountered when producing large area thin films by solution-processing methods based on the deposition of nanoparticles are the following: (i) The formation of cracks due to the high deposition rates and the volume reduction associated with the organics removal. (ii) The poor crystallinity of the as-deposited precursor films, which require a posterior thermal treatment. (iii) The organics used during material synthesis and ink formulation and the residual carbon left after their thermal decomposition strongly deteriorate the film electronic properties and block its crystallization.

A multistrategy approach to overcome these limitations is presented here. We used a custom-made automated pulsed spray deposition system to produce CZTS films from colloidal CZTS nanoparticles having carefully adjusted compositions and organic free surfaces. Organic ligands used during nanoparticle synthesis were displaced by an antimony salt. We demonstrate here the effectiveness of these approaches to produce highly homogeneous, organic- and crack-free films. These films were annealed in a Se atmosphere to obtain CZTSe absorber layers. We further demonstrate that the Sb-based ligand exchange strategy not only eliminates carbon from the final film, thus improving electrical conductivity, but also strongly promotes crystal growth before Sb is completely removed from the film.

CZTS nanoparticles were prepared by the reaction of copper, tin and zinc salts with tetraethylthiouram disulfide in the presence of octadecylphosphonic acid (ODPA) and oleylamine (OLA). We believe OLA controls the nanoparticle growth and its stability. On the other hand, ODPA allows a better control of composition by coordinating with the precursor salts and facilitating their incorporation into the final crystal structure. ODPA does not remain attached to the nanoparticle surface, thus it was easily removed during the purification process and only OLA remained as an organic impurity.

Figure 1 shows representative TEM and HRTEM micrographs of the ~25 ± 5 nm CZTS nanoparticles produced by this procedure (see Supporting Information, SI). Composition could be tuned by changing the amount of precursors in the initial solution. Taking into account that highest CZTSe solar cell efficiencies were obtained from copper-poor and zinc-rich CZTSe,[1,3] to study ligand exchange procedures, crystallization and selenization processes and to fabricate CZTSe solar cells, we produced CZTS nanoparticles with the composition $Cu_{1.9}Zn_{1.1}Sn_{1.0}S_{4.0}$, as measured by EDX.

Even when organic ligands can be decomposed by an annealing process, their carbon footprint still limits the device performance and blocks the crystal growth.[4] Furthermore, cracks are usually formed when removing organics after deposition. Therefore, to produce solar cell grade thin films,

Received: July 5, 2013
Published: October 12, 2013

   dx.doi.org/10.1021/ja4068639 | J. Am. Chem. Soc. 2013, 135, 15982−15985

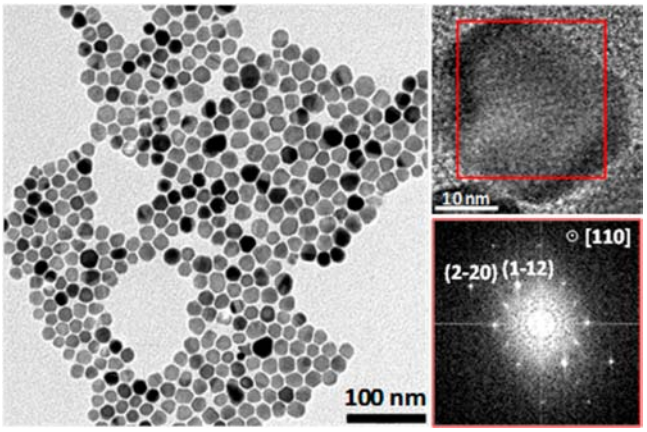

Figure 1. TEM and HRTEM micrograph, and power spectrum analysis of CZTS nanoparticles.

organics need to be displaced from the nanoparticle surface before deposition.

However, to process the materials in solution and to obtain homogeneous films, nanoparticles need to be soluble in a liquid carrier. Thus, either we use thick solvents and binders that keep nanoparticles dispersed during long enough times, which will again leave large amounts of carbon after decomposition, or we replace the organic ligands used during the synthesis by shorter but still effective stabilizers.[5] In this last direction, inorganic salts are excellent candidates to displace organic ligands and render the nanoparticles soluble in low boiling point solvents that after deposition can be easily evaporated without a carbon footprint. The use of inorganic salts gives also the opportunity to tune the final film composition or to introduce external dopants that control the material electronic properties.[6] While we chose to control the film composition at the nanoparticle synthesis stage, we tested multiple ligand exchange agents looking for the one that did not change the film composition but helped its crystallization. Among the different salts tested, best results were obtained for $SbCl_3$.

OLA displacement with $SbCl_3$ was carried out using a biphase system (Figure 2). We mixed in a 2:1 ratio a 0.1 M

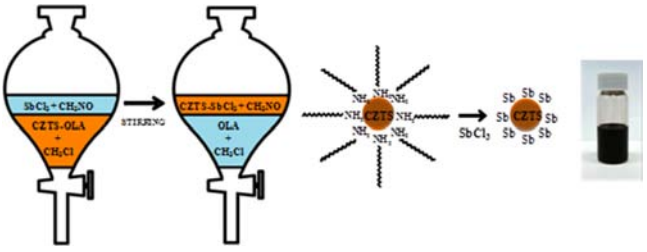

Figure 2. Schematized view of the procedure followed for the OLA displacement with $SbCl_3$.

$SbCl_3$ solution in formamide with a 10 g/L solution of nanoparticles in chloroform. Then, the solution was vigorously shaken until nanoparticles transferred to the formamide phase. The formamide solution was afterward washed several times with chloroform to drag all remaining organic ligands. Nanoparticles were finally precipitated with acetonitrile and redispersed in *N*,*N*-dimethylformamide (DMF) at a 5 g/L concentration. As a reference, we also replaced OLA with a relatively more conventional species, $(NH_4)_2S$, using a similar procedure. $(NH_4)_2S$ ligand exchange was performed by adding 1 mL of a 20 wt % $(NH_4)_2S$ solution in water and 10 mL of formamide into a 10 mL of a 10 g/L solution of CZTS nanoparticles in chloroform.

Figure 3b shows the mass loss as a function of temperature for CZTS-OLA, CZTS-$SbCl_3$ and CZTS-$(NH_4)_2S$ nano-

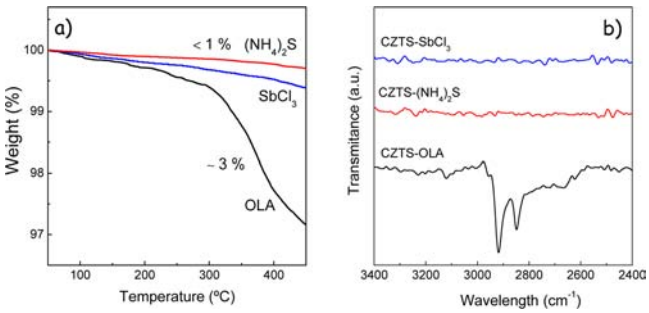

Figure 3. (a) TGA and (b) ATR-FTIR spectra from CZTS-OLA, CZTS-$SbCl_3$ and CZTS-$(NH_4)_2S$ nanoparticles.

particles. A relative mass decrease of a 3% was measured for purified CZTS-OLA nanocrystals when heated to 450 °C under a nitrogen flow. On the other hand, after $(NH_4)_2S$ and $SbCl_3$ ligand exchange, nanocrystals showed a mass loss of less than 1% associated to the evaporation of S, Sb and probably Sn. The higher mass loss measured for CZTS-OLA nanoparticles was consistent with the thermal decomposition of the bulky OLA molecules, which were not present at the surface of CZTS-$SbCl_3$ and CZTS-$(NH_4)_2S$ nanoparticles.

Figure 3c shows the ATR-FTIR spectra of dried CZTS-OLA, CZTS-$SbCl_3$ and CZTS-$(NH_4)_2S$ nanoparticles. The CZTS-OLA spectrum showed the C−H vibration modes in the high-frequency region (2800−3000 cm^{-1}) characteristic of OLA. This feature disappeared from the CZTS-$SbCl_3$ and CZTS-$(NH_4)_2S$ spectra.

The carbon left after annealing CZTS nanoparticles in a nitrogen atmosphere was measured by CHN quantitative elemental analysis. A 3% of carbon was obtained from the analysis of annealed CZTS-OLA nanoparticles. On the other hand, the carbon percentage measured from annealed CZTS-$SbCl_3$ and CZTS-$(NH_4)_2S$ nanoparticles was below the detection limit of our system: ~ 0.1%.

After organic ligand displacement and purification, CZTS-$SbCl_3$ and CZTS-$(NH_4)_2S$ nanoparticles were stable in solution during times long enough to allow their spray deposition.

A custom-made pulsed spray-deposition system was used to produce CZTS nanoparticle-based thin films from a 5 g/L CZTS solution in DMF. The system consisted of a heated sample holder and a nozzle that used nitrogen as the carrier gas. A computer-controlled electrovalve was used to create the spray pulses. The number of pulses, the pulse time, the time between pulses, and the substrate temperature were precisely controlled through a computer. The optimized process to produce homogeneous 2 μm-thick CZTS films was 40 cycles of 0.5 s pulses with a pulse-to-pulse time of 60 s, and a substrate temperature of 160 °C. For the crystallization analysis and to fabricate solar cells, CZTS nanoparticles were sprayed onto 2 × 2 cm^2 molybdenum-coated soda-lime glass substrates in air.

To produce solar cell grade layers, CZTS films were annealed for 60 min in a Se and Sn-rich atmosphere. A complete substitution of S by Se took place during selenization, transforming the precursor kesterite CZTS film (JCPDS 00-026-0575, Figure 4a) into kesterite CZTSe (JCPDS 01-070-

dx.doi.org/10.1021/ja4068639 | J. Am. Chem. Soc. 2013, 135, 15982−15985

8930, Figure 4b). A partial selenization of the Mo bottom layer was also observed.

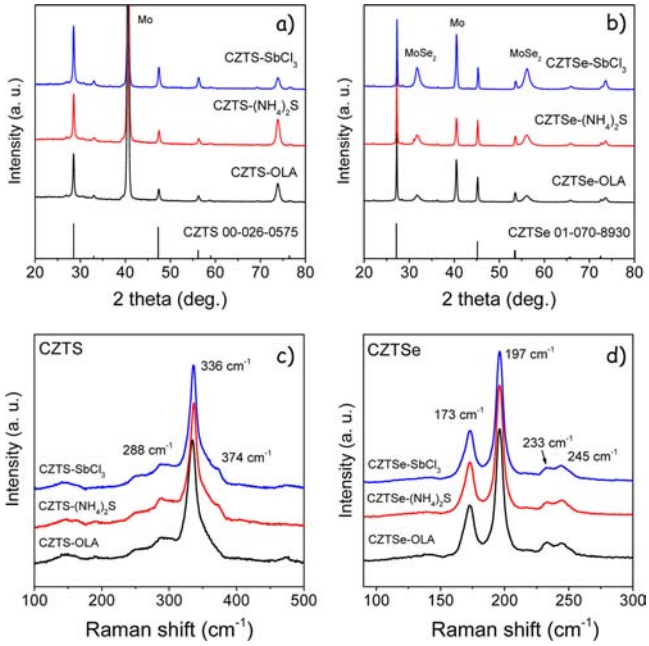

Figure 4. XRD patterns (a,b) and Raman spectra (c,d) of as-deposited (a,c) and 550 °C selenized (b,d) films prepared from CZTS-OLA, CZTS-$SbCl_3$ and CZTS-$(NH_4)_2S$ nanoparticles.

Raman spectra were measured with 514.5 nm excitation wavelength having a penetration depth of backscattered light below 100 nm (Figure 4c,d). The precursor film exhibited the typical Raman spectrum of CZTS nanocrystalline layers with broad peaks (fwhm of 13−14 cm^{-1}) at 288 and 336 cm^{-1} and a shoulder at 374 cm^{-1} corresponding to the two main A symmetry modes and likely to a B symmetry mode of the CZTS kesterite structure.[7,8] After annealing, and independently of the ligand, the crystalline quality of the films was largely improved (fwhm of main A peak = 5.5−6.5 cm^{-1}). CZTSe films showed a peak at 173 cm^{-1} which has been recently attributed to two A modes, the main A mode at 197 cm^{-1}, and two weaker peaks at around 233 cm^{-1} related to E/B symmetry modes.[7] No secondary phases were detected by either XRD or Raman measurements. Raman characterization using UV excitation (λ = 325 nm) also discarded the presence of ZnS.

Figure 5 shows cross-sectional SEM images of the precursor films and the films selenized at different temperatures, from 475 to 575 °C. Absorbers crystallized from CZTS-OLA and CZTS-$(NH_4)_2S$ films exhibited a typical bilayer structure formed by a bottom layer with fine grains and a top layer with larger crystals. Conversely, the absorbers crystallized from CZTS-$SbCl_3$ nanoparticles showed a single layer structure with large crystals covering from the substrate to the surface. Films obtained from CZTS-$SbCl_3$ nanoparticles systematically showed significantly larger crystal domain sizes than the ones produced from CZTS-$(NH_4)_2S$ and CZTS-OLA nanoparticles and even at temperatures below 500 °C relatively large crystal domains, in the micrometer range, were obtained.

Surprisingly, no Sb was detected after crystallization at temperatures above 500 °C. No peak shift or additional band was observed in the Raman spectra or the XRD patterns and no Sb was detected in the composition analysis performed by

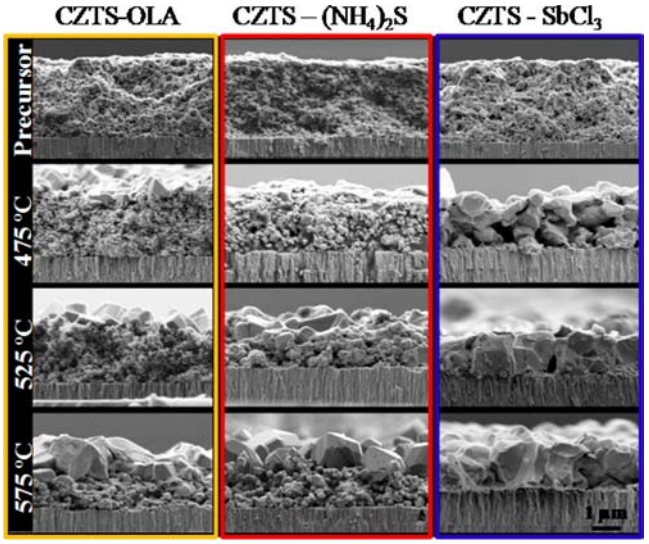

Figure 5. Cross-sectional SEM images of the CZTS precursor and CZTSe films prepared from CZTS-OLA, CZTS-$SbCl_3$ and CZTS-$(NH_4)_2S$ nanoparticles and annealed at temperatures from 475 to 575 °C.

EDX, ICP and XPS. EDX and ICP analyses showed the films to be copper-poor and zinc-rich, conserving the nanoparticles composition, both before (Cu/(Zn + Sn) = 0.85 and Zn/Sn = 1.09) and after crystallization (Cu/(Zn + Sn) = 0.81 and Zn/Sn = 1.01). Additionally, EDX showed an Sb content of about 5% for the CZTS-$SbCl_3$ thin films before selenization, but no Sb was detected on the CZTSe-$SbCl_3$ films after the heat treatment. ICP analyses showed an 8% by mass of Sb in the CZTS-$SbCl_3$ film before selenization, but no Sb after selenitzation. As-deposited CZTS-$SbCl_3$ films showed intense XPS Sb $3d_{5/2}$ and $3d_{3/2}$ peaks, corresponding to an atomic 20% Sb composition, but the crystallized CZTSe-$SbCl_3$ films showed no Sb-related peak (Figure SI3). Just an oxygen peak corresponding to a slight surface oxidation of the materials was detected by XPS in the crystallized but air exposed layers (Figure SI3). These results suggest that Sb did not incorporate to the bulk CZTSe crystals but it evaporated during the selenization process.

The use of Sb to promote crystal growth in Cu(In,Ga)Se_2 films was previously reported, but its role remains unclear.[9] We hypothesize that Sb incorporated to the CZTSe structure at the crystal surface locally forming a low melting point Sb-based chalcogenide. Various are the Sb-containing compounds with diamond-like phases that could be locally formed, e.g. Cu_3SbSe_4 with a melting temperatures of 425 °C[10] or even the quinary phase $CuZnSn_2Sb_3Se$,[11] although none of these were detected by XRD or Raman. Even in a substoichiometric ratio, the incorporation of Sb to the crystal structure could locally reduce the material's melting point, increasing its ionic mobility and its capacity for mass transfer and reorganization. We believe the decrease of the ion diffusion energy associated with Sb chemical incorporation ultimately promoted the diffusion-controlled crystallization process. As crystals domains grew, Sb was displaced to their surface where it accumulated. As crystallization proceeded, Sb evaporated and after 1 h at temperatures above 500 °C, no Sb was left within the CZTSe film.

Solar cells were fabricated from CZTS-$SbCl_3$ films deposited on 2 × 2 cm^2 soda-lime glass substrates with 800 nm of magnetron-sputtered Mo and selenized at 575 °C. A 60 nm

dx.doi.org/10.1021/ja4068639 | J. Am. Chem. Soc. 2013, 135, 15982−15985

thick CdS buffer layer was deposited by chemical bath deposition. To complete the device, a 50 nm layer of i-ZnO and a 250 nm layer of In_2O_3:Sn were grown by pulsed DC-magnetron sputtering.[3] Finally, samples were scribed to 3 × 3 mm^2 cells. Figure 6a shows a characteristic $J-V$ curve obtained

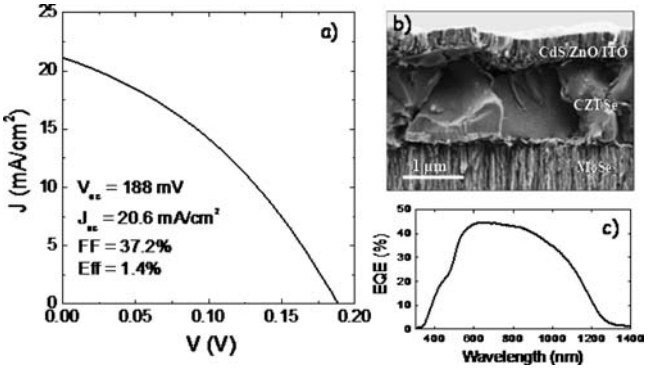

Figure 6. (a) Photovoltaic performance of a CZTSe solar cell prepared from the spray deposition of CZTS-$SbCl_3$ nanoparticles. (b) Cross-sectional SEM image of the device. (c) External quantum efficiency spectral response of the same device.

under AM1.5 illumination from one of the devices. In a first optimization, devices with relatively high current density of 20 mA/cm^2 were systematically achieved. However, rather low open circuit voltages close to 200 mV and fill factors below 40% were measured. This translated into power conversion efficiencies of 1.4% that although modest are encouraging for this low-cost and high-yield technology that allows the absorber material deposition in air and with the use of no hazardous chemicals, nor high vacuum equipment.

The device spectral response showed external quantum efficiencies up to 45% and allowed to calculate a band gap of 0.97 eV (Figure 6c). EQE showed a relatively high degree of recombination at the space charge region, suggesting that the improvement of the junction could help to increase efficiency. Indeed, we believe the moderate performances measured could be related with a poor CZTSe-CdS interface, which also reduced the device open circuit voltage and fill factor.

In summary, a ligand exchange strategy to remove organics, introduce antimony and render CZTS nanoparticles in solution and an automated pulsed spray deposition system to produce homogeneous and crack-free thin films were presented. Their combination allowed obtaining carbon-free thin films with controlled thickness and composition. The incorporation of Sb to the crystal surfaces locally reduced the material melting point promoting the diffusion-controlled crystallization. While thus-prepared CZTSe devices require optimization, our results demonstrate that the multistrategy approach presented here has a high potential to produce low-cost photovoltaic grade CZTSe layers.

■ ASSOCIATED CONTENT

Supporting Information

Synthesis and characterization details, complementary SEM micrographs, solar cell performance results and XPS spectra. This material is available free of charge via the Internet at http://pubs.acs.org.

■ AUTHOR INFORMATION

Corresponding Author

acabot@irec.cat

Notes

The authors declare no competing financial interest.

■ ACKNOWLEDGMENTS

This work was supported by the European Regional Development Funds and the Framework 7 program under project SCALENANO (FP7-NMP-ENERGY-2011-284486). E.S. thanks the Spanish government for the "Ramon y Cajal" fellowship (RYC-2011-09212).

■ REFERENCES

(1) (a) Todorov, T. K.; Reuter, K. B.; Mitzi, D. B. *Adv. Mater.* **2010**, *22*, E156. (b) Todorov, T. K.; Tang, J.; Bag, S.; Gunawan, O.; Gokmen, T.; Zhu, Y.; Mitzi, D. B. *Adv. Energy Mater.* **2013**, *3*, 34. (c) Guo, Q.; Ford, G. M.; Yang, W.-C.; Walker, B. C.; Stach, E. A.; Hillhouse, H. W.; Agrawal, R. *J. Am. Chem. Soc.* **2010**, *132*, 17384.

(2) (a) Shavel, A.; Arbiol, J.; Cabot, A. *J. Am. Chem. Soc.* **2010**, *132*, 4514. (b) Shavel, A.; Cadavid, D.; Ibáñez, M.; Carrete, A.; Cabot, A. *J. Am. Chem. Soc.* **2012**, *134*, 1438. (c) Ibáñez, M.; Zamani, R.; Li, W.; Shavel, A.; Arbiol, J.; Morante, J. R.; Cabot, A. *Cryst. Growth Des.* **2012**, *12*, 1085. (d) Ibáñez, M.; Zamani, R.; Lalonde, A.; Cadavid, D.; Li, W.; Shavel, A.; Arbiol, J.; Morante, J. R.; Gorsse, S.; Snyder, G. J.; Cabot, A. *J. Am. Chem. Soc.* **2012**, *134*, 4060. (e) Ibáñez, M.; Cadavid, D.; Zamani, R.; García-Castelló, N.; Izquierdo-Roca, V.; Li, W.; Fairbrother, A.; Prades, J. D.; Shavel, A.; Arbiol, J.; Pérez-Rodríguez, A.; Morante, J. R.; Cabot, A. *Chem. Mater.* **2012**, *24*, 562. (f) Singh, A.; Geaney, H.; Laffir, F.; Ryan, K. M. *J. Am. Chem. Soc.* **2012**, *134*, 2910. (g) Aldakov, D.; Lefrancois, A.; Reiss, P. *J. Mater. Chem. C* **2013**, *1*, 3756.

(3) Fairbrother, A.; García-Hemme, E.; Izquierdo-Roca, V.; Fontané, X.; Pulgarín-Agudelo, F. A.; Vigil-Galán, O.; Pérez-Rodríguez, A.; Saucedo, E. J. *Am. Chem. Soc.* **2012**, *134*, 8018.

(4) Ibáñez, M.; Zamani, R.; Li, W.; Cadavid, D.; Gorsse, S.; Katcho, N. A.; Shavel, A.; López, A. M.; Morante, J. R.; Arbiol, J.; Cabot, A. *Chem. Mater.* **2012**, *24*, 4615.

(5) (a) Kovalenko, M. V.; Scheele, M.; Talapin, D. V. *Science* **2009**, *324*, 1417. (b) Nag, A.; Kovalenko, M. V.; Lee, J.-S.; Liu, W.; Spokoyny, B.; Talapin, D. V. *J. Am. Chem. Soc.* **2011**, *133*, 10612.

(6) Cadavid, D.; Ibáñez, M.; Shavel, A.; Dura, O. J.; Lopez de la Torre, M. A.; Cabot, A. *J. Mater. Chem. A* **2013**, *1*, 4864.

(7) (a) Khare, A.; Himmetoglu, B.; Johnson, M.; Norris, D. J.; Cococcioni, M.; Aydil, E. S. *J. Appl. Phys.* **2012**, *111*, 083707. (b) Gürel, T.; Sevik, C.; Çağın, T. *Phys. Rev. B* **2011**, *84*, 205201. (c) Fontané, X.; Izquierdo-Roca, V.; Saucedo, E.; Schorr, S.; Yukhymchuk, V. O.; Valakh, M. Y.; Pérez-Rodríguez, A.; Morante, J. R. *J. Alloys Compd.* **2012**, *539*, 190. (d) Fontané, X.; Calvo-Barrio, L.; Izquierdo-Roca, V.; Saucedo, E.; Pérez-Rodriguez, A.; Morante, J. R.; Berg, D. M.; Dale, P. J.; Siebentritt, S. *Appl. Phys. Lett.* **2011**, *98*, 181905. (e) Djemour, R.; Redinger, A.; Mousel, M.; Gütay, L.; Fontané, X.; Izuierdo-Roca, V.; Pérez-Rodríguez, A.; Siebentritt, S. *Opt. Express* **2013**, *21*, A695.

(8) Espindola-Rodriguez, M.; Placidi, M.; Vigil-Galán, O.; Izquierdo-Roca, V.; Fontané, X.; Fairbrother, A.; Sylla, D.; Saucedo, E.; Pérez-Rodríguez, A. *Thin Solid Films* **2013**, *535*, 67.

(9) (a) Zhang, S.; Wu, L.; Yue, R.; Yan, Z.; Zhan, H.; Xiang, Y. *Thin Solid Films* **2013**, *527*, 137. (b) Yuan, M.; Mitzi, D. B.; Gunawan, O.; Kellock, A. J.; Chey, S. J.; Deline, V. R. *Thin Solid Films* **2010**, *519*, 852. (c) Yuan, M.; Mitzi, D. B.; Liu, W.; Kellock, A. J.; Chey, S. J.; Deline, V. R. *Chem. Mater.* **2010**, *22*, 285.

(10) Berger, L. I.; Prochukhan, V. D. *Ternary Diamond-like Semiconductors*; Consultants Bureau: New York, 1969, 64.

(11) Pamplin, B. *Prog. Cryst. Growth Charact.* **1981**, 3.